

Pyramid transforms via nonstationary subdivision schemes

Hadar Landau^{*1}, Wael Mattar^{†1}, and Nir Sharon^{‡1}

¹School of Mathematical Sciences, Tel Aviv University, Tel Aviv, Israel

Abstract

Pyramid transforms are constructive methods for analyzing sequences in a multiscale fashion. Traditionally, these transforms rely on stationary upsampling and downsampling operations. In this paper, we propose employing nonstationary subdivision schemes as upsampling operators that vary according to the refinement level. These schemes offer greater flexibility, enabling the development of advanced multiscale transforms, including geometric multiscale analysis. We establish the fundamental properties of these nonstationary operators and demonstrate their effectiveness in capturing and analyzing geometric features. In particular, we present applications to highlight their utility in detecting geometric structures in planar objects.

1 Introduction

Multiscale transforms are essential tools in signal and image processing, enabling a hierarchical mathematical analysis of objects. Customarily, the first scale in the transform corresponds to a coarse representation, and as scales increase, so do the levels of approximation [6, 23]. The pyramid transform uses a refinement or upsampling operator together with a corresponding decimation operator for the construction of a fast multiscale representation of signals in a classical setting that goes back to [9, 26]. The simplicity of this powerful method opened the door for numerous applications and extensions, such as in geophysics [21], data compression [22], scientific computing [18], fluid mechanics [7], and geometry [27], just to name a few.

Subdivision schemes are computationally efficient tools for producing smooth objects from discrete sets of points [10]. These schemes are defined by iteratively applying their subdivision operators that refine discrete sets. If a subdivision scheme relies on the same operator at each level of refinement, then it is said to be stationary. Otherwise, it is nonstationary. The subdivision refinements, whether stationary or not, that serve as upsampling operators in the context of pyramid transforms, give rise to a natural connection to multiscale representations [2, 6].

Multiscale transforms, based upon subdivision operators, commonly use interpolating subdivision schemes, i.e., operations that preserve the coarse objects through their refinements. The interpolation simplifies the process of calculating the missing detail coefficients across different scales. Particularly, coefficients associated with the interpolating values are systematically zeroed, and do not have to be saved or processed in the following analysis levels. Recently, the concept of multiscale transforms using subdivision operators has been extended to include noninterpolating subdivision schemes [17]. The primary challenge in constructing a noninterpolating pyramid transform centers on calculating the multiscale details. In particular, given a noninterpolating subdivision scheme, the corresponding downsampling operators involve applying infinitely supported real-valued sequences. Therefore, care must be taken when realizing and implementing these operators [24, 25].

This paper focuses on pyramid transforms that use nonstationary subdivision schemes. Nonstationary subdivision schemes offer significant advantages over their stationary counterparts, primarily due to their enhanced flexibility and approximation capabilities. For example, unlike stationary schemes that are limited to reproducing polynomial functions, nonstationary schemes can reproduce more general polynomial functions such as trigonometric, hyperbolic, or exponential. This property is beneficial for analyzing oscillatory signals, such as speech signals and other band-limited signals in general, or accurately modeling shapes like conic sections and spirals, or for applications involving the solutions of differential equations [3, 5]. Additionally, the level-dependent nature of nonstationary schemes enables better control over smoothness and geometric features. However, this increased flexibility comes at the cost of greater mathematical and computational complexity, particularly in analyzing convergence and regularity [13, 15]. Despite these challenges, nonstationary schemes

^{*}Email: hadarlandau1@mail.tau.ac.il

[†]Corresponding author: waelmattar@mail.tau.ac.il

[‡]Email: nsharon@tauex.tau.ac.il

provide a powerful tool when the limitations of stationary schemes are insufficient for the modeling task at hand.

The primary contributions of this paper lie in the introduction and analysis of a novel framework for nonstationary pyramids. First, we formulate a general class of nonstationary pyramids, extending the classical notion to accommodate level-dependent refinement rules. We then rigorously derive and establish essential theoretical properties of these pyramids, including their coefficient decay and stability characteristics. Finally, we demonstrate the practical applicability of the proposed framework by introducing a quantitative measure that assesses how closely a given planar curve approximates a circle, thus highlighting the effectiveness of nonstationary pyramids in geometric analysis and shape approximation.

The structure of the paper is as follows. Section 2 provides the necessary background and notation, including a concise overview of subdivision schemes and pyramid constructions. In Section 3, we introduce the nonstationary framework, present the formal definitions, and establish key properties of nonstationary pyramids. Section 4 illustrates the applicability of the proposed framework through geometry-driven pyramids and demonstrates their use in quantifying how closely planar curves resemble circles. Finally, Section 5 summarizes the main findings and outlines potential directions for future research.

2 Subdivision schemes and pyramid transforms

This section establishes the foundational definitions and notation required for the developments that follow.

2.1 Subdivision schemes

Throughout the paper, real-valued sequences will be denoted by bold letters. A linear univariate subdivision scheme \mathcal{S} acts on a real-valued bi-infinite sequence $\mathbf{c} = \{c_j \in \mathbb{R} \mid j \in \mathbb{Z}\}$. Applying the subdivision scheme on \mathbf{c} returns a sequence $\mathcal{S}(\mathbf{c})$, which we associate with the values of the refined grid $2^{-1}\mathbb{Z}$. By repeating this process infinitely many times, and associating the results on finer and finer nesting grids, we get values that are associated with the dyadic rationals $\{j/2^k : (k, j) \in \mathbb{N} \times \mathbb{Z}\}$, which is a dense subset of the real line. A subdivision scheme is termed *convergent* if for any bounded sequence \mathbf{c} , the limit $\mathcal{S}^\infty(\mathbf{c})$ converges uniformly at the dyadic rationals to the values of some continuous function, see [11] for convergence analysis. A linear subdivision scheme with a finitely supported mask α is denoted by \mathcal{S}_α , and is given explicitly by

$$\mathcal{S}_\alpha(\mathbf{c})_j = \sum_{i \in \mathbb{Z}} \alpha_{j-2i} c_i, \quad j \in \mathbb{Z}. \quad (1)$$

The refinement rule (1) can be rewritten with two rules depending on the parity of the index j . Namely,

$$\mathcal{S}_\alpha(\mathbf{c})_{2j} = \sum_{i \in \mathbb{Z}} \alpha_{2i} c_{j-i} \quad \text{and} \quad \mathcal{S}_\alpha(\mathbf{c})_{2j+1} = \sum_{i \in \mathbb{Z}} \alpha_{2i+1} c_{j-i}, \quad j \in \mathbb{Z}. \quad (2)$$

Moreover, the scheme (1) can be written as the convolution $\mathcal{S}_\alpha(\mathbf{c}) = \alpha * (\mathbf{c} \uparrow 2)$, where \uparrow is the simple upsampling operator

$$(\mathbf{c} \uparrow 2)_j = \begin{cases} c_{j/2}, & j = 2k, \quad k \in \mathbb{Z}, \\ 0, & j = 2k+1, \quad k \in \mathbb{Z}. \end{cases} \quad (3)$$

A subdivision scheme is termed *interpolating* if $\mathcal{S}_\alpha(\mathbf{c})_{2j} = c_j$ for all $j \in \mathbb{Z}$, or alternatively $\mathcal{S}_\alpha(\mathbf{c}) = \mathbf{c} \uparrow 2$ over the even indices, for any sequence \mathbf{c} . A necessary condition for the convergence of a subdivision scheme with the refinement rule (1), see e.g. [10], is

$$\sum_{i \in \mathbb{Z}} \alpha_{2i} = \sum_{i \in \mathbb{Z}} \alpha_{2i+1} = 1. \quad (4)$$

With this condition, the rules (2) can be interpreted as *center of masses*. All subdivision schemes considered in this paper are assumed to be convergent.

2.2 Pyramids for data analysis

2.2.1 Multiscale transform based on interpolating linear refinement

The notion of pyramid transforms is constituted by representing a high-resolution sequence of data points as a pyramid structure composed of a coarse approximation along with layers of details, each associated with a different scale (see, e.g., [17, 19]). For a review of interpolating multiscale transforms, refer to [9, 20].

Let \mathcal{S}_α be an interpolating subdivision scheme. A high-resolution sequence $\mathbf{c}^{(J)}$, $J \in \mathbb{N}$ associated with the fine grid $2^{-J}\mathbb{Z}$, can be recursively decomposed into a coarse (low-resolution) sequence $\mathbf{c}^{(0)}$ on the integer grid, along with a collection of detail coefficient sequences $\mathbf{d}^{(\ell)}$, $\ell = 1, \dots, J$, that are supported on the grids $2^{-\ell}\mathbb{Z}$ respectively. This is done by iterating

$$\mathbf{c}^{(\ell-1)} = \mathbf{c}^{(\ell)} \downarrow 2, \quad \mathbf{d}^{(\ell)} = \mathbf{c}^{(\ell)} - \mathcal{S}_\alpha \mathbf{c}^{(\ell-1)}, \quad \ell = 1, \dots, J, \quad (5)$$

where the downsampling operator $\downarrow 2$ is defined by $(\mathbf{c} \downarrow 2)_j = c_{2j}$ for all $j \in \mathbb{Z}$. This recursive process produces a pyramid of sequences given by $\{\mathbf{c}^{(0)}; \mathbf{d}^{(1)}, \dots, \mathbf{d}^{(J)}\}$. The synthesis, i.e., the reconstruction of the original sequence, is obtained through the iterative scheme

$$\mathbf{c}^{(\ell)} = \mathcal{S}_\alpha \mathbf{c}^{(\ell-1)} + \mathbf{d}^{(\ell)}, \quad \ell = 1, \dots, J, \quad (6)$$

which serves as the inverse transform of (5).

By the construction of the pyramid (5), it is easy to see that the detail coefficient $d_j^{(\ell)}$ at some $j \in \mathbb{Z}$ and $\ell = 1, \dots, J$ encodes the difference between the true data point $c_j^{(\ell)}$ and the refinement outcome $(\mathcal{S}_\alpha \mathbf{c}^{(\ell-1)})_j$. Furthermore, because \mathcal{S}_α is interpolating, then $d_{2j}^{(\ell)} = 0$ for all $j \in \mathbb{Z}$. This property is overall written as the equation

$$[(\mathcal{I} - \mathcal{S}_\alpha \downarrow 2)\mathbf{c}^{(\ell)}] \downarrow 2 = \mathbf{0}, \quad \ell = 1, \dots, J, \quad (7)$$

where \mathcal{I} is the identity operator in the functional setting. This property is vital for many applications, including data compression, as it allows us to eliminate half of the detail coefficients when storing pyramid representations of real-valued sequences.

2.2.2 Multiscale transform based on approximating linear refinement

The main challenge in replacing \mathcal{S}_α with a noninterpolating one in the multiscale transform (5) is that the sequence $\mathcal{S}_\alpha(\mathbf{c})$ does not preserve the elements \mathbf{c} . In other words, property (7) is violated, and hence the detail coefficients at the even indices exhibit statistical significance, resulting in an ineffective pyramid representation. More precisely, more storage is required to store the pyramid than to store the sequence itself. However, the extension of multiscale transforms based on interpolating subdivision operators to a wider class of refinements is made possible with the introduction of *decimation* operators.

Decimation operators are designed to recover data points associated with even indices after one iteration of refinement. Given a subdivision operator \mathcal{S}_α , we look for an operator \mathcal{D} such that

$$[(\mathcal{I} - \mathcal{S}_\alpha \mathcal{D})\mathbf{c}] \downarrow 2 = \mathbf{0} \quad (8)$$

holds for any real-valued sequence \mathbf{c} . Technically, condition (8) is a generalization to condition (7) allowing more sophisticated downsampling operators. The generalization is simply done by replacing $\downarrow 2$ with the operator \mathcal{D} .

Let γ be a sequence such that $\sum_{i \in \mathbb{Z}} \gamma_i = 1$. Then, for any sequence \mathbf{c} we explicitly define the decimation operator \mathcal{D}_γ associated with the sequence γ to be

$$\mathcal{D}_\gamma(\mathbf{c})_j = \sum_{i \in \mathbb{Z}} \gamma_{j-i} c_{2i}, \quad j \in \mathbb{Z}. \quad (9)$$

Decimation operators serve as downscaling tools, reducing the number of data points when applied to a sequence. The sequence γ can have an infinite support, and therefore calculating (9) usually involves truncation errors. The decimation operator (9) can also be expressed as

$$\mathcal{D}_\gamma(\mathbf{c}) = \gamma * (\mathbf{c} \downarrow 2), \quad (10)$$

where $*$ denotes the convolution operator over \mathbb{Z} . Moreover, if $\gamma = \delta$ is the Kronecker delta sequence ($\delta_0 = 1$ and $\delta_i = 0$ for $i \neq 0$), then \mathcal{D}_δ reduces to simple downsampling $\downarrow 2$.

With a subdivision scheme \mathcal{S}_α at hand, equation (8) admits a unique solution, given by the decimation operator \mathcal{D}_γ , where γ is obtained from the convolutional equation

$$\gamma * (\alpha \downarrow 2) = \delta. \quad (11)$$

Using Wiener's Lemma, if $\alpha \downarrow 2$ is compactly supported, then such γ with infinite support exists. In this case we say that \mathcal{D}_γ is the *reverse* of \mathcal{S}_α . Furthermore, γ is bounded by

$$|\gamma_j| \leq C\lambda^{|j|}, \quad j \in \mathbb{Z}, \quad (12)$$

for constants $C > 0$ and $\lambda \in (0, 1)$. This geometric decay is crucial for the computation of \mathcal{D}_γ as we will see next.

We follow the same approximation methods presented in [25]. The decimation operator \mathcal{D}_γ can be approximated in practice via a proper truncation of its associated sequence. In particular, given a *truncation* parameter $\varepsilon > 0$, the truncation of γ is defined by

$$\tilde{\gamma}_j(\varepsilon) = \begin{cases} \gamma_j, & |\gamma_j| > \varepsilon \\ 0, & \text{otherwise} \end{cases}, \quad j \in \mathbb{Z}. \quad (13)$$

Indeed, the bound (12) guarantees that the support of $\tilde{\gamma}(\varepsilon)$ is finite for any positive ε . For convenience we omit the parameter ε from the notation. Consequently, $\tilde{\gamma}$ is normalized in the following sense

$$\zeta_j = \frac{\tilde{\gamma}_j}{\sum_{m \in \mathbb{Z}} \tilde{\gamma}_m}, \quad j \in \mathbb{Z}. \quad (14)$$

The normalization is essential for multiscaling as it directly affects the significance of the even detail coefficients, as shown in [25].

As follows from the above, given a noninterpolating subdivision scheme \mathcal{S}_α with its reverse decimation operator \mathcal{D}_ζ , associated with a normalized truncated mask ζ for some ε , and a sequence $\mathbf{c}^{(J)}$ associated with the values over the grid $2^{-J}\mathbb{Z}$, the noninterpolating multiscale transform is given by

$$\mathbf{c}^{(\ell-1)} = \mathcal{D}_\zeta \mathbf{c}^{(\ell)}, \quad \mathbf{d}^{(\ell)} = \mathbf{c}^{(\ell)} - \mathcal{S}_\alpha \mathbf{c}^{(\ell-1)}, \quad \ell = 1, \dots, J. \quad (15)$$

Iterating (15) yields a pyramid of data $\{\mathbf{c}^{(0)}; \mathbf{d}^{(1)}, \dots, \mathbf{d}^{(J)}\}$ as similar to the interpolating transform (5). We obtain synthesis again by (6). As shown in [25], the multiscale transform (15) enjoys two main properties, which are decay of the detail coefficients and stability of the inverse transform.

3 Pyramids based on nonstationary schemes

This section is devoted to nonstationary subdivision schemes, which are characterized by level-dependent refinement rules. We begin by introducing the necessary notation, which forms the basis for defining the nonstationary pyramid transform. This transform extends the classical stationary framework by incorporating varying subdivision operators at each level. To illustrate the construction and potential of this approach, two representative examples are presented.

3.1 nonstationary Subdivision Schemes

The refinement operator of a subdivision scheme can also be implemented in a level-dependent way, that is to say, by using different masks at different iterations. Denote by $\{\alpha^{(k)} \mid k \in \mathbb{N}\}$ the sequence of finite sets of real coefficients identifying, for each k , the k -level mask of a nonstationary subdivision scheme. We then denote through $\mathbf{S} = \{\mathcal{S}_{\alpha^{(k)}} \mid k \in \mathbb{N}\}$ the sequence of linear subdivision operators based on the above masks to obtain the nonstationary subdivision scheme:

$$\mathbf{f}^{(k)} = \mathcal{S}_{\alpha^{(k)}} \mathbf{f}^{(k-1)} \quad \text{where} \quad (\mathcal{S}_{\alpha^{(k)}} \mathbf{f}^{(k-1)})_i = \sum_{j \in \mathbb{Z}} \alpha_{i-2j}^{(k)} f_j^{(k-1)}, \quad k \in \mathbb{N}, \quad (16)$$

starting from an initial sequence $\mathbf{f}^{(0)} = \{f_i \in \mathbb{R}, i \in \mathbb{Z}\}$.

Note that, whenever the recursive relation in (16) relies on the same mask at each level of refinement, namely $\alpha^{(k)} = \alpha^{(1)}$ for all $k \geq 2$, then the subdivision scheme is said to be stationary.

Let the result of the first k recursive operations of a subdivision scheme on the initial data $\mathbf{f}^{(0)}$ be denoted by $\mathbf{f}^{(k)} = \mathbf{S}^k \mathbf{f}^{(0)} = \mathcal{S}_{\alpha^{(k)}} \cdots \mathcal{S}_{\alpha^{(1)}} \mathbf{f}^{(0)}$. We say that the scheme \mathbf{S} converges if for any initial data $\mathbf{f}^{(0)}$, there exists $f \in C^m$, for some fixed $m \geq 0$, such that

$$\lim_{k \rightarrow \infty} \sup_{j \in \mathbb{Z}} |f(2^{-k}j) - f_j^{(k)}| = 0. \quad (17)$$

In this case we denote $\mathbf{S}^\infty \mathbf{f}^{(0)} = f$, and we say that the scheme is C^m .

Remark 3.1. Two additional comments:

1. For brevity, the refinement rule in (16) is defined in the linear setting. However, the overall framework readily accommodates non-linear variants as well. In particular, adaptations for manifold-valued data are feasible, in line with existing approaches in the literature (see, e.g., [16]).
2. From a practical standpoint, nonstationary subdivision schemes are not significantly more complex than their stationary counterparts, particularly given that only a limited number of refinement levels are typically applied in real-world applications.

Nonstationary subdivision schemes exhibit distinct properties and expand the class of subdivision limit functions. For example, when applied to 2-D points, they can generate circles, ellipses, or other conic sections. Additionally, they enable users to modify the shape of a subdivision limit using level-dependent tension parameters. In the univariate case, they can generate exponential B-splines [13], C^∞ functions with compact support as the Rvachev-type function [14], or B-spline-like functions with higher smoothness relative to the support size [1, 4].

Here are examples of two nonstationary subdivision schemes, taken from [15] and [3], respectively.

Example 3.2. This is a nonstationary generalization of the interpolatory 4-point Dubuc–Deslauriers scheme, which generates circles. The refinement rules are

$$\begin{aligned} f_{2j}^{(k)} &= f_j^{(k-1)}, \\ f_{2j+1}^{(k)} &= \frac{-1}{16 \cos^2(\theta 2^{-k-1}) \cos(\theta 2^{-k})} (f_{j-1}^{(k-1)} + f_{j+2}^{(k-1)}) + \frac{(1 + 2 \cos(2\theta 2^{-k+1}))^2}{16 \cos^2(\theta 2^{-k-1}) \cos(\theta 2^{-k})} (f_j^{(k-1)} + f_{j+1}^{(k-1)}), \end{aligned} \quad (18)$$

where θ is a scaling factor. When $\theta = 0$, we obtain the celebrated 4-point interpolatory scheme based on polynomials [12, 8]. Alternatively, these insertion rules tend to the 4-point insertion rules as k approaches infinity. A worth mentioning value is $\theta = \frac{2\pi}{N}$, where applying the rules to the equidistributed points on the circle with radius R and center at the origin, $\{f_j = R(\cos(j\theta), \sin(j\theta))\}_{j=1}^N$, it generates a denser set of points on the circle.

Example 3.3. This is a nonstationary generalization of the cubic B-spline scheme, which generates exponential splines. The refinement rules are

$$\begin{aligned} f_{2j}^{(k)} &= \frac{1}{2(v^{(k)} + 1)^2} f_{j-1}^{(k-1)} + \frac{4(v^{(k)})^2 + 2}{2(v^{(k)} + 1)^2} f_j^{(k-1)} + \frac{1}{2(v^{(k)} + 1)^2} f_{j+1}^{(k-1)}, \\ f_{2j+1}^{(k)} &= \frac{2v^{(k)}}{(v^{(k)} + 1)^2} f_j^{(k-1)} + \frac{2v^{(k)}}{(v^{(k)} + 1)^2} f_{j+1}^{(k-1)}, \end{aligned} \quad (19)$$

where the nonstationary parameter $v^{(k)}$ is defined as

$$v^{(k)} = \frac{1}{2} (e^{i \frac{\theta}{2^{k+1}}} + e^{-i \frac{\theta}{2^{k+1}}}) = \sqrt{\frac{1 + v^{(k-1)}}{2}}, \quad k \geq 0, \quad v^{(-1)} > -1. \quad (20)$$

Customarily, $v^{(-1)}$ is set to $\cos(\theta)$ where as before, θ is a parameter related to the sampling rate. When $\theta = 0$, then $v^{(k)} = 1$ for all k and the refinement rules coincide with the ones of the cubic B-spline. This is also the case as k tends to infinity.

3.2 Pyramids based on nonstationary schemes

Pyramid transforms can be implemented in a level-dependent manner by utilizing nonstationary subdivision schemes. In particular, multiscaling a real-valued sequence $\mathbf{c}^{(J)}$ with a nonstationary family of subdivision schemes $\{\mathcal{S}_{\alpha^{(\ell)}} \mid \ell = 1, \dots, J\}$ is defined by

$$\mathbf{c}^{(\ell-1)} = \mathcal{D}_{\gamma^{(\ell)}} \mathbf{c}^{(\ell)}, \quad \mathbf{d}^{(\ell)} = \mathbf{c}^{(\ell)} - \mathcal{S}_{\alpha^{(\ell)}} \mathbf{c}^{(\ell-1)}, \quad \ell = 1, \dots, J, \quad (21)$$

where $\mathcal{D}_{\gamma^{(\ell)}}$ is the decimation operator corresponding to $\mathcal{S}_{\alpha^{(\ell)}}$. That is, the pair $\gamma^{(\ell)}$ and $\alpha^{(\ell)}$ solve (11). Conversely, the synthesis is obtained by iterating

$$\mathbf{c}^{(\ell)} = \mathcal{S}_{\alpha^{(\ell)}} \mathbf{c}^{(\ell-1)} + \mathbf{d}^{(\ell)}, \quad \ell = 1, \dots, J. \quad (22)$$

We illustrate the nonstationary pyramid in Figure 1.

Although we use a different decimation operator at each decomposition iteration, we truncate the sequences $\gamma^{(\ell)}$, $\ell = 1, \dots, J$ with a uniform truncation threshold ε . The truncated sequences are then normalized to obtain $\zeta^{(\ell)}$ as appears in (14). The shift invariant sequences then replace $\gamma^{(\ell)}$ in (21). We proceed with two examples and discuss the nonstationary pyramid transforms that correspond to Examples 3.2 and 3.3.

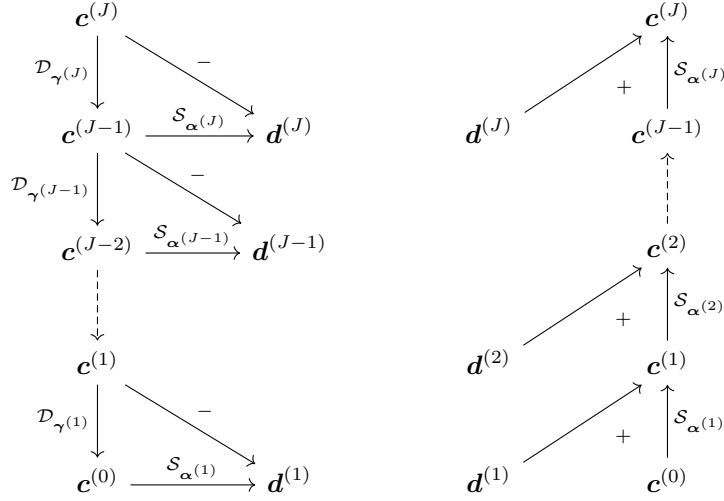


Figure 1: The pyramid transform. On the left is the analysis (21), and on the right is the synthesis (22).

Example 3.4. The subdivision scheme (18) is interpolating, and its even refinement rule is actually stationary. Therefore, the downscaling operators $\mathcal{D}_{\gamma(\ell)}$, $\ell = 1, \dots, J$, simply reduce to the downsampling operator $\downarrow 2$, and hence $\mathbf{c}^{(\ell-1)}$ of the nonstationary multiscaling (21) is computed as in (5).

Example 3.5. In this example, we focus on the refinement rules given in (19), which are noninterpolating. Consequently, the associated decimation operators $\mathcal{D}_{\gamma(\ell)}$, for $\ell = 1, \dots, J$, correspond to sequences with infinite support. Notably, as the level ℓ increases, the decimation operator $\mathcal{D}_{\gamma(\ell)}$ asymptotically approaches the cubic B-spline decimation. This behavior follows from the continuity of the solution to (11) with respect to the refinement mask of the subdivision scheme. The first four coefficients of the decimation sequence are illustrated in Figure 2.

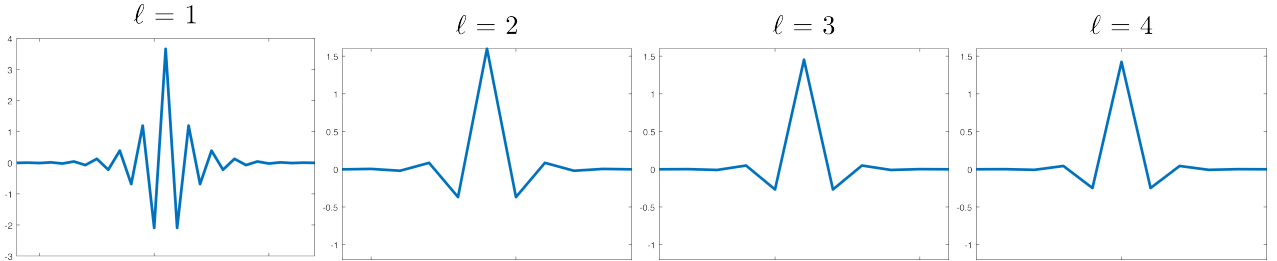


Figure 2: The first four decimation coefficients correspond to the nonstationary subdivision scheme defined in (19). For each level ℓ , the decimation operator is obtained by solving (11), followed by truncation at a fixed threshold $\varepsilon = 10^{-15}$ and subsequent normalization. A notable difference is observed between the first and second operators, while the remaining ones display similar profiles and progressively tend toward the (stationary) cubic B-spline decimation operator.

It turns out that stationary and nonstationary transforms share similar properties. Let us now present the decay of the details and the stability theorems for the nonstationary case. The following results and their proofs are analogous to those shown in [25] and [17].

Theorem 3.6 (Details coefficients decay). *Let $f : \mathbb{R} \rightarrow \mathbb{R}$ be a differentiable and bounded function, and let $\mathbf{c}^{(J)}$, $J \in \mathbb{N}$ be its samples over the dyadic grid $2^{-J}\mathbb{Z}$, that is, $\mathbf{c}^{(J)} = f|_{2^{-J}\mathbb{Z}}$. Let $\{\mathcal{S}_{\alpha(\ell)}, \ell = 1, \dots, J\}$ be a family of nonstationary subdivision schemes, and $\{\mathcal{D}_{\zeta(\ell)}, \ell = 1, \dots, J\}$ its corresponding family of decimation operator associated with shift invariant sequences $\zeta^{(\ell)}$. Then the detail coefficients obtained by the multiscale transform (21) satisfy*

$$\|\mathbf{d}^{(\ell)}\|_{\infty} \leq \left(K_{\alpha(\ell), \zeta^{(\ell)}} \cdot \|f'\|_{\infty} \cdot \|\zeta^{(\ell)}\|_1^{-1} \cdot \prod_{m=\ell}^J \|\zeta^{(m)}\|_1 \right) 2^{-\ell}, \quad \ell = 1, \dots, J, \quad (23)$$

where $K_{\alpha^{(\ell)}, \zeta^{(\ell)}} = K_{\zeta^{(\ell)}} \|\alpha^{(\ell)}\|_1 + K_{\alpha^{(\ell)}} \|\zeta^{(\ell)}\|_1$, and $K_c = 2 \sum_{i \in \mathbb{Z}} |c_i| |i|$ for any finitely supported sequence \mathbf{c} .

Proof. We first show that $\|\mathbf{d}^{(\ell)}\|_\infty$ is proportional to $\Delta \mathbf{c}^{(\ell)}$ for all levels $\ell = 1, \dots, J$, namely

$$\|\mathbf{d}^{(\ell)}\|_\infty \leq K_{\alpha^{(\ell)}, \zeta^{(\ell)}} \Delta \mathbf{c}^{(\ell)}. \quad (24)$$

To this end, we start with an evaluation of a general term in $\mathbf{d}^{(\ell)}$. Observe

$$\begin{aligned} d_k^{(\ell)} &= c_k^{(\ell)} - \sum_i \alpha_{k-2i}^{(\ell)} c_i^{(\ell-1)} = \sum_i \alpha_{k-2i}^{(\ell)} (c_k^{(\ell)} - c_i^{(\ell-1)}) = \sum_i \alpha_{k-2i}^{(\ell)} \left(c_k^{(\ell)} - \sum_n \zeta_{i-n}^{(\ell)} c_{2n}^{(\ell)} \right) = \\ &= \sum_i \alpha_{k-2i}^{(\ell)} \left(\sum_n \zeta_{i-n}^{(\ell)} c_k^{(\ell)} - \sum_n \zeta_{i-n}^{(\ell)} c_{2n}^{(\ell)} \right) = \sum_i \alpha_{k-2i}^{(\ell)} \left(\sum_n \zeta_{i-n}^{(\ell)} (c_k^{(\ell)} - c_{2n}^{(\ell)}) \right). \end{aligned}$$

Consequently,

$$\begin{aligned} |d_k^{(\ell)}| &\leq \sum_i |\alpha_{k-2i}^{(\ell)}| \left(\sum_n |\zeta_{i-n}^{(\ell)}| \cdot |c_k^{(\ell)} - c_{2n}^{(\ell)}| \right) \\ &\leq \sum_i |\alpha_{k-2i}^{(\ell)}| \left(\sum_n |\zeta_{i-n}^{(\ell)}| \cdot |2n - k| \cdot \Delta \mathbf{c}^{(\ell)} \right) \\ &\leq \sum_i |\alpha_{k-2i}^{(\ell)}| \left(\sum_n |\zeta_{i-n}^{(\ell)}| \cdot (|2n - 2i| + |2i - k|) \right) \cdot \Delta \mathbf{c}^{(\ell)} \\ &\leq \sum_i |\alpha_{k-2i}^{(\ell)}| \left(K_{\zeta^{(\ell)}} + |2i - k| \|\zeta^{(\ell)}\|_1 \right) \cdot \Delta \mathbf{c}^{(\ell)} \\ &= \left(K_{\zeta^{(\ell)}} \|\alpha^{(\ell)}\|_1 + K_{\alpha^{(\ell)}} \|\zeta^{(\ell)}\|_1 \right) \cdot \Delta \mathbf{c}^{(\ell)}. \end{aligned}$$

Applying the supremum over $k \in \mathbb{Z}$ on the latter inequality gives (24). We now evaluate the term $\Delta \mathbf{c}^{(\ell)}$ for an arbitrary ℓ based on the assumption that $\mathbf{c}^{(J)}$ is sampled from f on the equispaced grid $2^{-J}\mathbb{Z}$. Since f is bounded and differentiable, then on the finest level we have that

$$\Delta \mathbf{c}^{(J)} \leq 2^{-J} \|f'\|_\infty. \quad (25)$$

This inequality is guaranteed by the Mean Value Theorem. In particular, for any $k \in \mathbb{Z}$ there exists a point x_k in the open interval connecting the two consecutive grid points $k2^{-J}$ and $(k+1)2^{-J}$, such that $|c_{k+1}^{(J)} - c_k^{(J)}| \leq 2^{-J} |f'(x_k)|$, and hence (25) is obtained by taking the supremum over the index k . On coarser levels however, since Δ commutes with the convolution operator, by (10) we get the recursive relation

$$\Delta \mathbf{c}^{(\ell-1)} = \Delta(\zeta^{(\ell)} * (\mathbf{c}^{(\ell)} \downarrow 2)) \leq \|\zeta^{(\ell)}\|_1 \cdot \Delta(\mathbf{c}^{(\ell)} \downarrow 2) \leq 2 \|\zeta^{(\ell)}\|_1 \cdot \Delta \mathbf{c}^{(\ell)}, \quad (26)$$

which holds for $\ell = 1, \dots, J$. Finally, iterative calculations of (26) involving (25) and (24) yield (23). \square

Under the assumption that the analyzed input sequence $\mathbf{c}^{(J)}$ is sampled from a differentiable function, Theorem 3.6 guarantees that the detail coefficients obtained by the nonstationary transform (21) exhibit a decay of factor 2 with each decomposition level. Furthermore, in the particular case where the subdivision schemes are stationary, then the constant $K_{\alpha^{(\ell)}, \zeta^{(\ell)}}$ in (23) becomes level-independent, and the product therein becomes $\|\zeta\|_1^{J-\ell}$. The overall outcome then coincides with Corollary 3.5 in [25].

Let us now show that the inverse multiscale transform (22) is stable.

Theorem 3.7 (Stability of the reconstruction). *Let $\{\mathbf{c}^{(0)}, \mathbf{d}^{(1)}, \dots, \mathbf{d}^{(J)}\}$ and $\{\tilde{\mathbf{c}}^{(0)}, \tilde{\mathbf{d}}^{(1)}, \dots, \tilde{\mathbf{d}}^{(J)}\}$ be two multiscale representations obtained by (21) with some family of nonstationary subdivision schemes $\{\mathcal{S}_{\alpha^{(\ell)}}, \ell = 1, \dots, J\}$. Assume that there exists a constant $M > 0$ such that $\max_{\ell=1, \dots, J} \|\mathcal{S}_{\alpha^{(\ell)}}\|_\infty \leq M$. Then the reconstructed data $\mathbf{c}^{(J)}$ and $\tilde{\mathbf{c}}^{(J)}$ via (22), applied on the two pyramids respectively, obey*

$$\|\mathbf{c}^{(J)} - \tilde{\mathbf{c}}^{(J)}\|_\infty \leq L \left(\|\mathbf{c}^{(0)} - \tilde{\mathbf{c}}^{(0)}\|_\infty + \sum_{\ell=1}^J \|\mathbf{d}^{(\ell)} - \tilde{\mathbf{d}}^{(\ell)}\|_\infty \right), \quad (27)$$

where $L = M^J$ if $M > 1$, else $L = 1$.

Proof. By the linearity of subdivision schemes (1) and the reconstruction formula (22) we iteratively get

$$\begin{aligned}
\|\mathbf{c}^{(J)} - \tilde{\mathbf{c}}^{(J)}\|_\infty &= \|\mathcal{S}_{\alpha^{(J)}}(\mathbf{c}^{(J-1)} - \tilde{\mathbf{c}}^{(J-1)}) + (\mathbf{d}^{(J)} - \tilde{\mathbf{d}}^{(J)})\|_\infty \\
&= \|\mathcal{S}_{\alpha^{(J)}}\mathcal{S}_{\alpha^{(J-1)}}(\mathbf{c}^{(J-2)} - \tilde{\mathbf{c}}^{(J-2)}) + \mathcal{S}_{\alpha^{(J)}}(\mathbf{d}^{(J-1)} - \tilde{\mathbf{d}}^{(J-1)}) + (\mathbf{d}^{(J)} - \tilde{\mathbf{d}}^{(J)})\|_\infty \\
&\vdots \\
&= \left\| \prod_{\ell=1}^J \mathcal{S}_{\alpha^{(\ell)}}(\mathbf{c}^{(0)} - \tilde{\mathbf{c}}^{(0)}) + \sum_{\ell=1}^J \prod_{m=\ell+1}^J \mathcal{S}_{\alpha^{(m)}}(\mathbf{d}^{(\ell)} - \tilde{\mathbf{d}}^{(\ell)}) \right\|_\infty \\
&\leq \left\| \prod_{\ell=1}^J \mathcal{S}_{\alpha^{(\ell)}} \right\|_\infty \|\mathbf{c}^{(0)} - \tilde{\mathbf{c}}^{(0)}\|_\infty + \sum_{\ell=1}^J \left\| \prod_{m=\ell+1}^J \mathcal{S}_{\alpha^{(m)}} \right\|_\infty \|\mathbf{d}^{(\ell)} - \tilde{\mathbf{d}}^{(\ell)}\|_\infty \\
&\leq L \left(\|\mathbf{c}^{(0)} - \tilde{\mathbf{c}}^{(0)}\|_\infty + \sum_{\ell=1}^J \|\mathbf{d}^{(\ell)} - \tilde{\mathbf{d}}^{(\ell)}\|_\infty \right).
\end{aligned}$$

The last inequality is true because the operator norm is submultiplicative. We note here that the products in the proof denote the decomposition of refinement operators, while the second product slightly abuses the notation for the sake of a compact expression. \square

It is known that if a family of nonstationary subdivision schemes is asymptotically equivalent to a convergent subdivision scheme, like the ones presented in Examples 3.2 and 3.3, then the necessary condition $\max_{\ell=1,\dots,J} \|\mathcal{S}_{\alpha^{(\ell)}}\|_\infty \leq M$ is satisfied for some $M > 0$, see [14]. Moreover, we remark here that the explicit formula for computing the operator norm of the subdivision scheme $\mathcal{S}_{\alpha^{(\ell)}}$ is given by

$$\|\mathcal{S}_{\alpha^{(\ell)}}\|_\infty = \max \left\{ \sum_{k \in \mathbb{Z}} |\alpha_{2k}^{(\ell)}|, \sum_{k \in \mathbb{Z}} |\alpha_{2k+1}^{(\ell)}| \right\}. \quad (28)$$

Theorem 3.7 ensures that small perturbations in the pyramid representation of a sequence lead to proportionate changes in the subsequent synthesis. This stability property is essential for various applications, including denoising and contrast enhancement, where one typically modifies the detail coefficients before reconstruction, see for example [25, 24]. Conversely, the following theorem shows the stability of the decomposition.

First, we evaluate the operator norm of a decimation operator (9). Given a decimation operator \mathcal{D}_ζ associated with a shift-invariant mask ζ , its operator norm is given by

$$\|\mathcal{D}_\zeta\|_\infty = \sup_{\|\mathbf{c}\|_\infty \leq 1} \|\zeta * (\mathbf{c} \downarrow 2)\|_\infty = \|\zeta\|_1. \quad (29)$$

Because the elements of ζ sum to one, then we have $\|\mathcal{D}_\zeta\|_\infty \geq 1$ for any shift-invariant mask ζ .

Theorem 3.8 (Stability of the decomposition). *Let $\mathbf{c}^{(J)}$ and $\tilde{\mathbf{c}}^{(J)}$ be two bounded sequences, and let $\{\mathcal{S}_{\alpha^{(\ell)}}\}$, $\ell = 1, \dots, J$ be a family of nonstationary subdivision schemes. Denote by $\{\mathcal{D}_{\zeta^{(\ell)}}\}$, $\ell = 1, \dots, J$ its corresponding family of decimation operators associated with shift invariant sequences $\zeta^{(\ell)}$. Then*

$$\|\mathbf{c}^{(0)} - \tilde{\mathbf{c}}^{(0)}\|_\infty \leq \prod_{m=1}^J \|\zeta^{(m)}\|_1 \cdot \|\mathbf{c}^{(J)} - \tilde{\mathbf{c}}^{(J)}\|_\infty, \quad (30)$$

and

$$\|\mathbf{d}^{(\ell)} - \tilde{\mathbf{d}}^{(\ell)}\|_\infty \leq \left(\|\mathcal{I} - \mathcal{S}_{\alpha^{(\ell)}}\mathcal{D}_{\zeta^{(\ell)}}\|_\infty \cdot \|\zeta^{(\ell)}\|_1^{-1} \cdot \prod_{m=\ell}^J \|\zeta^{(m)}\|_1 \right) \|\mathbf{c}^{(J)} - \tilde{\mathbf{c}}^{(J)}\|_\infty, \quad \ell = 1, \dots, J, \quad (31)$$

where $\{\mathbf{c}^{(0)}, \mathbf{d}^{(1)}, \dots, \mathbf{d}^{(J)}\}$ and $\{\tilde{\mathbf{c}}^{(0)}, \tilde{\mathbf{d}}^{(1)}, \dots, \tilde{\mathbf{d}}^{(J)}\}$ are the multiscale representations (21) of $\mathbf{c}^{(J)}$ and $\tilde{\mathbf{c}}^{(J)}$, respectively.

Proof. By the linearity of the operators involved in the multiscaling (21), and by (29) we can easily see that

$$\|\mathbf{c}^{(\ell-1)} - \tilde{\mathbf{c}}^{(\ell-1)}\|_\infty = \|\mathcal{D}_{\zeta^{(\ell)}}(\mathbf{c}^{(\ell)} - \tilde{\mathbf{c}}^{(\ell)})\|_\infty \leq \|\zeta^{(\ell)}\|_1 \|\mathbf{c}^{(\ell)} - \tilde{\mathbf{c}}^{(\ell)}\|_\infty, \quad (32)$$

for all $\ell = 1, \dots, J$, and hence (30) is immediately obtained. Equivalently, the detail coefficients satisfy

$$\|\mathbf{d}^{(\ell)} - \tilde{\mathbf{d}}^{(\ell)}\|_\infty = \|(\mathcal{I} - \mathcal{S}_{\alpha^{(\ell)}}\mathcal{D}_{\zeta^{(\ell)}})(\mathbf{c}^{(\ell)} - \tilde{\mathbf{c}}^{(\ell)})\|_\infty \leq \|\mathcal{I} - \mathcal{S}_{\alpha^{(\ell)}}\mathcal{D}_{\zeta^{(\ell)}}\|_\infty \|\mathbf{c}^{(\ell)} - \tilde{\mathbf{c}}^{(\ell)}\|_\infty.$$

Therefore, by combining the latter evaluation with (32) we get (31). \square

Naturally, the results of Theorem 3.8 agree with Theorem 11 in [17] when the family of subdivision schemes is stationary. Furthermore, the distance $\|\mathbf{c}^{(0)} - \tilde{\mathbf{c}}^{(0)}\|_\infty$ appearing in (30) depends solely on the decay factor of the decimation coefficients in theory, and on the threshold of truncation ε in practice. In particular, the faster the decay of the elements of $\zeta^{(\ell)}$, the lower $\|\zeta^{(\ell)}\|_1$ tends to become, and therefore a lower distance between the coarse approximations is achieved. In the particular case where the multiscaling (21) is interpolating, taking us back to (5), then $\zeta^{(\ell)} = \delta$ and $\|\mathcal{D}_{\zeta^{(\ell)}}\|_\infty = 1$. This is the lowest value possible for this operator, which may lead to equality in (30).

Another valuable insight stemming from (31) is the following. First, observe the relation

$$\|[\mathcal{I} - \mathcal{S}_{\alpha^{(\ell)}} \mathcal{D}_{\zeta^{(\ell)}}(\cdot)] \downarrow 2\|_\infty \leq \|\mathcal{I} - \mathcal{S}_{\alpha^{(\ell)}} \mathcal{D}_{\zeta^{(\ell)}}\|_\infty,$$

where the operator in the left hand side appears in (8), and its operator norm is equivalent to the residual of the convolutional equation (11), namely $\|\delta - (\alpha \downarrow 2) * \zeta\|_1$, which measures how well ζ and α satisfy the equation. This equivalence follows from Theorem 4 in [17] and its proof. Consequently, choosing a bigger truncation threshold ε leads to a higher residual in (11), implying that the resulting detail coefficients will be less similar.

4 Geometric driven pyramids and their applications

Until now, we have demonstrated how to construct the pyramid using a nonstationary upsampling operator, even in the absence of guaranteed interpolation. However, the practical relevance of this construction may not yet be fully apparent. In this section, we present several concrete constructions that highlight the applicability of the framework from a geometric perspective.

All figures and examples presented in this section are available as open-source code to support reproducibility and can be accessed at: <https://github.com/HadarLandau/NSP>.

4.1 Reproducing exponential polynomials: The refinement

We start by defining spaces of exponential polynomials. Let $T \in \mathbb{Z}_+$, $\lambda = (\lambda_0, \lambda_1, \dots, \lambda_T)$ with $\lambda_T \neq 0$, be a finite set of real numbers, and let $D^n = d^n/dx^n$ be the n th order differentiation operator. We denote by $V_{T,\lambda}$ the space of exponential polynomials

$$V_{T,\lambda} = \left\{ f: \mathbb{R} \rightarrow \mathbb{C}, f \in C^T(\mathbb{R}) \mid \sum_{j=0}^T \lambda_j D^j f = 0 \right\}. \quad (33)$$

Define $\lambda(z) = \sum_{j=0}^T \lambda_j z^j$ and let $\{\theta_l, \tau_l\}_{l=1,\dots,N}$ be the set of zeros with multiplicities of $\lambda(z)$,

$$\lambda^{(r)}(\theta_l) = 0, \quad \text{where } r = 0, \dots, \tau_l - 1, \quad l = 1, \dots, N, \quad \tau_l \in \mathbb{N}, \quad T = \sum_{l=1}^N \tau_l. \quad (34)$$

Then, $V_{T,\lambda}$ is the subspace of dimension T of exponential polynomials of the form

$$V_{T,\lambda} = \text{Span}\{x^r e^{\theta_l x} : r = 0, \dots, \tau_l - 1, l = 1, \dots, N\}. \quad (35)$$

In the following, we provide the definition of a subdivision scheme that reproduces the space of exponential polynomials.

Definition 4.1 (Exponential reproduction). Let $\{\alpha^{(k)}(z) \mid k \geq 0\}$ be a sequence of subdivision symbols. This scheme is said to be reproducing exponentials if it is convergent, and for any $f \in V_{T,\lambda}$ and an initial sequence $\mathbf{f}^{(0)}$ uniformly sampled from f , it holds

$$\lim_{k \rightarrow \infty} \mathcal{S}_{\alpha^{(m+k)}} \mathcal{S}_{\alpha^{(m+k-1)}} \cdots \mathcal{S}_{\alpha^{(m)}} \mathbf{f}^{(0)} = f, \quad m \in \mathbb{N} \cup \{0\}. \quad (36)$$

Note that the property of exponential reproduction is independent of the starting level of refinement m .

We consider an example from [5] of a nonstationary subdivision scheme that reproduces the space

$$V_{T,\lambda} = \text{span}\{1, x, e^{tx}, e^{-tx}\},$$

which is suitable for representing conic sections. Depending on the value of the parameter t , this space captures different types of conics. For example, hyperbolic for $t = 1$, trigonometric for $t = i$, and purely polynomial for $t = 0$.

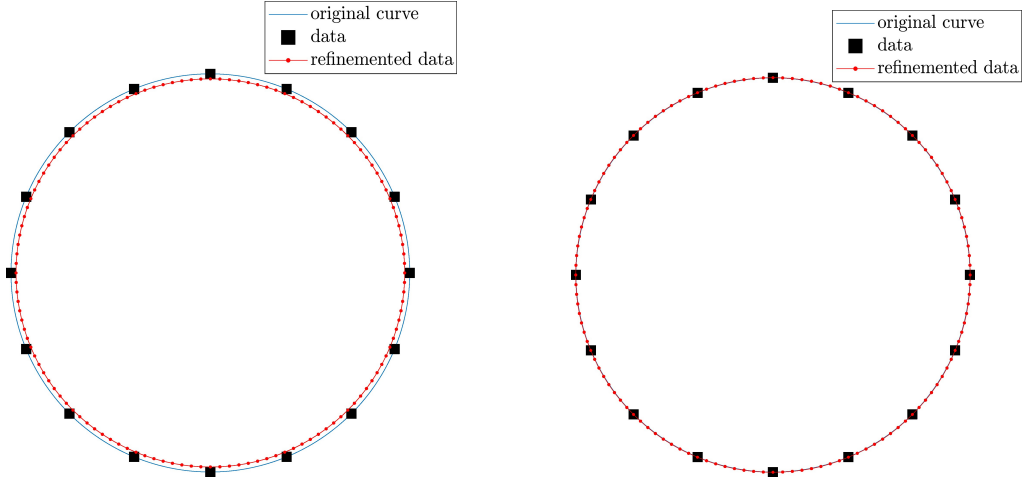


Figure 3: The figure compares refinement results for a circular shape using subdivision schemes. Original curves (blue), initial coarse points (black squares), and refined points (red dots) after three refinement steps are shown. The left plot, using the cubic B-spline scheme, provides an inaccurate approximation of the circle, whereas the right plot, using the geometric scheme (37), perfectly matches the original curve, highlighting its exponential reproduction property.

Example 4.2. The scheme $\mathcal{S}_{\alpha_1^{(k)}}$ is given by the refinement rules:

$$\begin{aligned} f_{2j}^{(k+1)} &= \frac{a^{(k)}}{4(v^{(k)} + 1)}(f_{j-2}^{(k)} + f_{j+2}^{(k)}) + \frac{1 + 2v^{(k)}(b^{(k)} + 2a^{(k)})}{4(v^{(k)} + 1)}(f_{j-1}^{(k)} + f_{j+1}^{(k)}) \\ &\quad + \frac{4v^{(k)}(1 - b^{(k)} - 2a^{(k)}) - 2a^{(k)} + 2}{4(v^{(k)} + 1)}f_j^{(k)}, \\ f_{2j+1}^{(k+1)} &= \frac{2a^{(k)}(v^{(k)} + 1) + b^{(k)}}{4(v^{(k)} + 1)}(f_{j-1}^{(k)} + f_{j+2}^{(k)}) + \frac{(2 - 2a^{(k)})(v^{(k)} + 1) - b^{(k)}}{4(v^{(k)} + 1)}(f_j^{(k)} + f_{j+1}^{(k)}). \end{aligned} \quad (37)$$

where

$$\begin{aligned} a^{(k)} &= \frac{(2 + \sqrt{2(v^{(k)} + 1)})(2 - v^{(k)}\sqrt{2(v^{(k)} + 1)})}{8v^{(k)}(v^{(k)} - 1)\sqrt{2(v^{(k)} + 1)}(v^{(k)} + 3 + 2\sqrt{2(v^{(k)} + 1)})}, \\ b^{(k)} &= \frac{(v^{(k)} + 1)(v^{(k)} - 2) - 2\sqrt{2(v^{(k)} + 1)}}{2v^{(k)}\sqrt{2(v^{(k)} + 1)}(v^{(k)} + 3 + 2\sqrt{2(v^{(k)} + 1)})}, \end{aligned} \quad (38)$$

with $v^{(k)} = \sqrt{\frac{1+v^{(k-1)}}{2}}$, $k \geq 0$ and $v^{(-1)} > -1$.

To determine the initial value, the initial data values are assumed to be equally spaced samples of a function $F \in V_{T,\lambda}$, $v^{(-1)}$ is chosen by

$$v^{(-1)} = \begin{cases} 1 & \text{if } F \text{ is purely polynomial,} \\ \cosh(\sigma) & \text{if } F \text{ is hyperbolic,} \\ \cos(\sigma) & \text{if } F \text{ is trigonometric,} \end{cases} \quad (39)$$

where σ is a positive number given by the spacing of the uniformly sampled points, i.e., $\sigma = 2\pi/N$, where N is the number of sample points.

The exponential reproduction property of the scheme of Example 4.2 is demonstrated in Figure 3. We began by sampling the unit circle, an example of a trigonometric polynomial, at nine equally spaced points. These samples were then refined over three levels using two schemes: the cubic B-spline scheme and the scheme of Example 4.2. As can be observed, the latter successfully reproduces the circle, maintaining the refined points precisely on the unit circle, while the cubic B-spline scheme yields points that drift away from the circle.

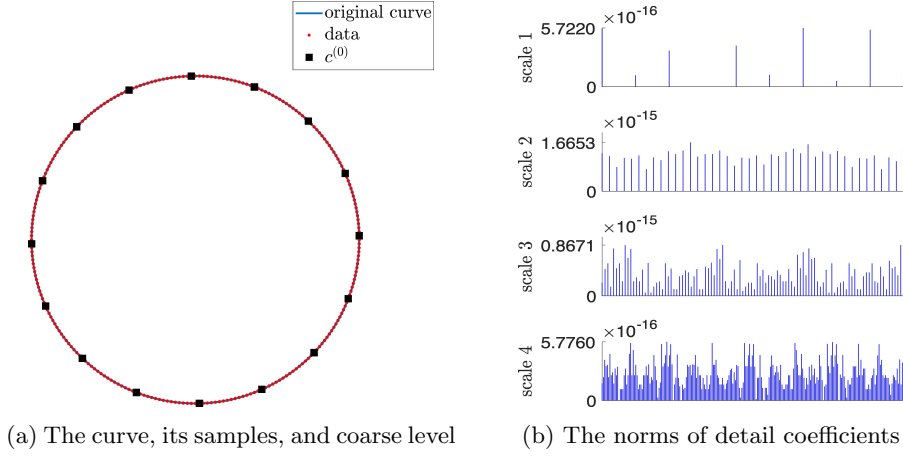


Figure 4: Points on the unit circle and their multiscale transform. On the left, 256 equispaced samples of the unit circle (in red), along with 16 data points (black squares) obtained by applying the analysis (21) four times. On the right, the Euclidean norms of the detail coefficients. Their values indicate that the initial samples indeed lie on a circle.

4.2 Application to circle detection: The pyramid

We proceed by deriving the pyramid transform that corresponds to the scheme in Example 4.2. To this end, we substitute $\alpha_1^{(k)}$ into (11) to determine the decimation operator for each level. Note that, in the subdivision scheme, $v^{(k)}$ is computed to match the number of samples, which doubles each time k increases. In contrast, during the decomposition process, the number of samples is halved at each level. Since the precise choice of $v^{(k)}$ is critical for preserving the reproducing properties of the scheme, this difference is addressed by choosing a new $v^{(-1)}$ at each level k , corresponds to the number of samples at that level and the first iteration of α_1 is set as $\alpha_1^{(k)}$. As before, we denote the k th level decimation operator that we calculate in (11) by $\gamma_1^{(k)}$. We truncate the decimation with $\varepsilon = 10^{-15}$ which gave rise to 33 nonzero coefficients and normalize each $\gamma_1^{(k)}$, see (13) and (14). Both $\alpha_1^{(k)}$ and $\zeta_1^{(k)}$ are substituted into (21) to compute $c^{(k-1)}$ and $d^{(k)}$.

Due to the scheme’s ability to reproduce conic sections and the locality of the subdivision operator, the resulting pyramid transform provides a potential tool for evaluating the circularity of a given set of samples. In this tool, we aim to analyze the multiscale representation of the data points for determining whether the points were sampled from a circle and, if not, estimate how closely the sampled shape resembles a circle. The following series of examples illustrates the practical validity of the proposed application. We generate several sets of samples drawn from the unit circle, each corrupted by varying levels and types of oscillatory noise, and analyze their circular structure, as reflected by the first four levels of their multiscale representations. In our first example, we present a clean planar circle in Figure 4a, sampled at 256 uniformly spaced points, along with its multiscale decomposition. The analysis process yields a coarse representation of 16 data points, which are also marked in this figure. On the right, Figure 4b presents the norms of the corresponding detail coefficients, as we recall that each coefficient is a planar vector. The effectively-zero norms of these coefficients, caused by machine precision limitations, confirm the exponential reproduction property, that is, the scheme’s ability to reproduce circles. Next, we present Figure 5, illustrating three examples of unit circles perturbed by oscillations of increasing magnitude from left to right. The bottom row shows the corresponding multiscale pyramid analysis for each case. As the magnitude of perturbations grows, the shape deviates further from a perfect circle, resulting in slower decay rates and larger magnitudes of detail coefficients at coarser levels. We also provide Figure 6 that presents a comparison, for each level ℓ , of the L_1 norm of the sequence of detail coefficients and the averaged L_2 norms of each detail coefficient, presented for the three cases. This comparison clearly and quantitatively indicates the above hierarchy of circle similarity.

Since the multiscale transform relies fundamentally on local operators, it is inherently sensitive to localized variations and irregularities in the underlying data. To illustrate this sensitivity explicitly, we conclude by demonstrating the efficacy of our geometric multiscale transform as an “anomaly detector.”

Anomaly detection in geometric settings, particularly in planar shapes, involves identifying shapes or sub-structures that deviate significantly from a learned notion of normality within a population of 2-D geometries, which, in our example, are sampled circles. Unlike point-based anomaly detection, our approach operates on a higher level and aims to locally detect any local topology that differs from the given geometry. We expect our

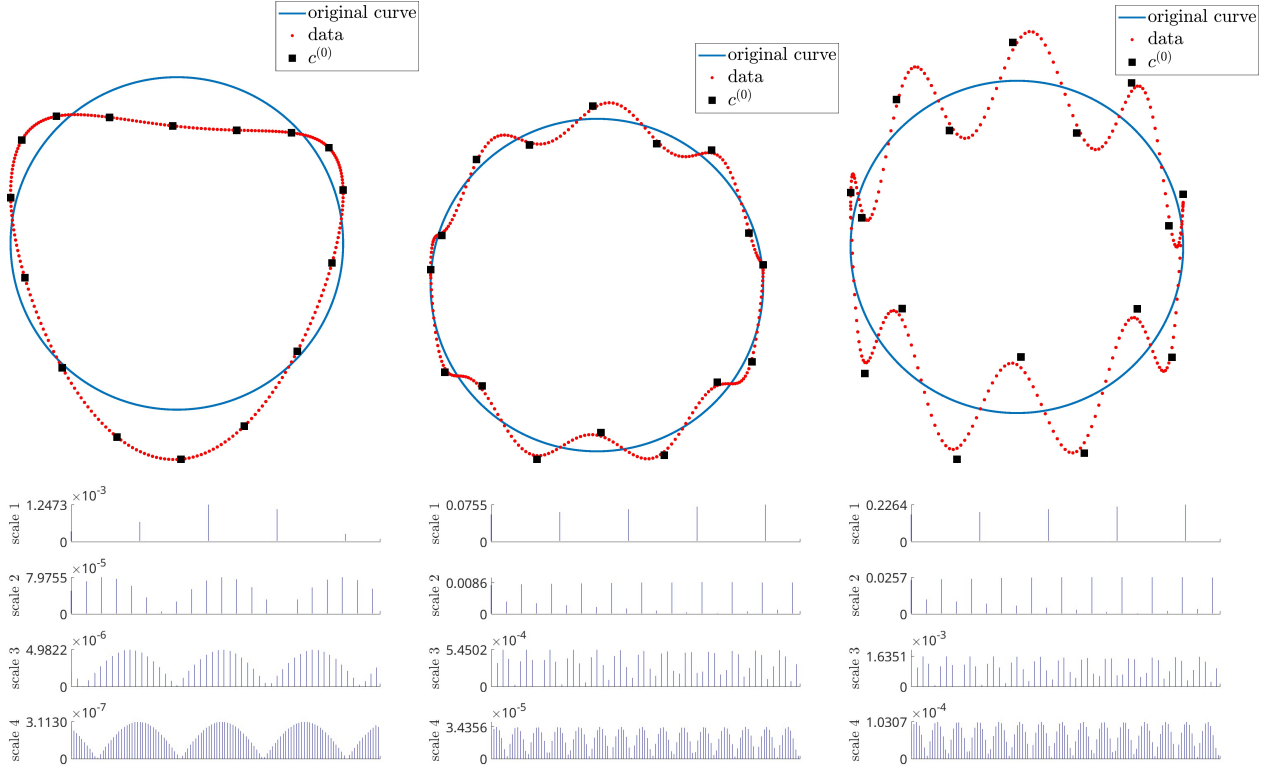


Figure 5: Quantifying similarity to a circular shape using multiscale transforms. Three examples of points sampled from perturbed circular curves (“wavy circles”) are shown. For each example, the upper plot displays 256 points along the curve and 16 coarse points (black squares) obtained after four decomposition steps of the transform. The lower plots illustrate the Euclidean norms of the corresponding detail coefficients. From left to right, perturbations increase, leading to larger detail coefficients. Smaller detail coefficients indicate greater similarity to a perfect circle.

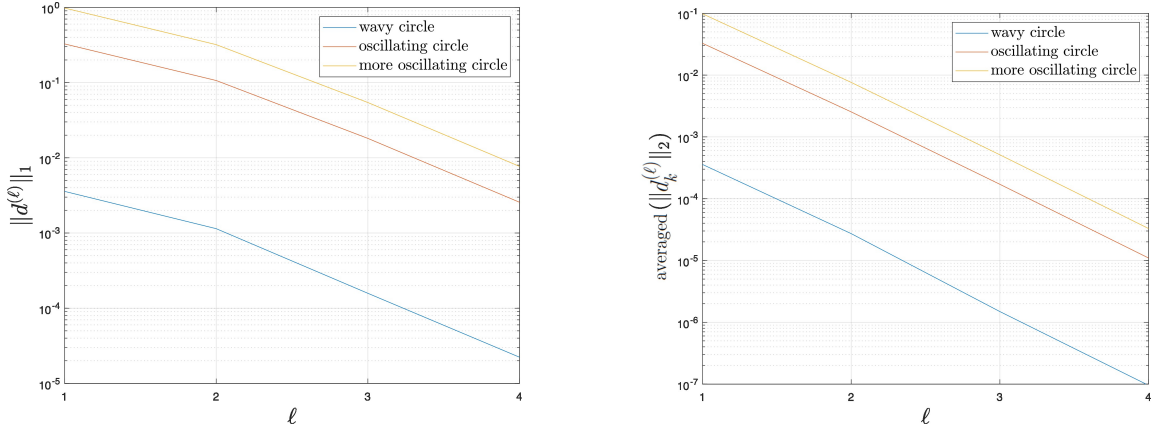


Figure 6: Log-scale plots of detail coefficients decay for three example shapes shown in Figure 5. The blue curve (“wavy circle”) corresponds to the leftmost shape, the red curve (“oscillating circle”) to the central shape, and the yellow curve (“highly oscillatory circle”) to the rightmost shape. The left panel shows the detail coefficients decay, measured by their L_1 -norm, indicating their magnitude and sparsity for each level $\ell = 1, \dots, 4$. The right panel shows the same decay, now measured by the averaged L_2 -norm, which quantifies the magnitude of each detail coefficient across each scale. Together, these two perspectives illustrate the hierarchical relationships among the examples revealed by the pyramid transform.

analysis to automatically indicate such an anomaly in a local and consistent fashion across the analysis level.

In Figure 7, we sample 256 equispaced points from a perfect circle to which we add a smooth, localized oscillatory perturbation confined to a single quadrant. Upon applying the multiscale decomposition to this

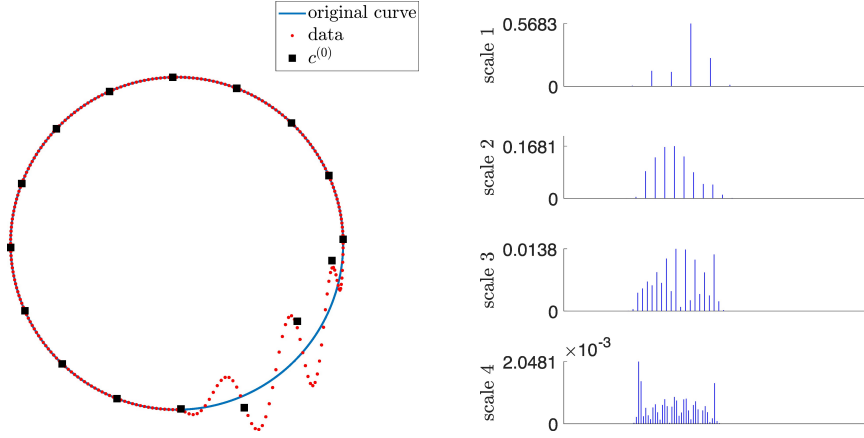


Figure 7: Anomaly detection in circles. On the left, 256 equispaced data points are sampled from a circle with a lower right quadrant perturbed by a localized smooth function. Overlaid are 16 coarse data points (black squares). On the right, the multiscale representation via the Euclidean norms of the detail coefficients. It can be clearly observed that the magnitude of the detail coefficients increases dramatically exactly in the region affected by perturbation.

modified dataset, we observe a clear differentiation in the resulting detail coefficients. Specifically, the coefficients corresponding to the perturbed quadrant become substantially larger compared to those in the unperturbed regions. These amplified coefficients clearly indicate that this particular region deviates significantly from circular geometry. In contrast, the coefficients from the unperturbed areas remain close to numerical zero (at double-precision accuracy). This stark distinction vividly illustrates the transform’s capability to detect, isolate, and characterize local irregularities, highlighting its intrinsic locality and exceptional spatial adaptivity.

5 Concluding remarks

In this paper, we have expanded the theory of pyramid multiscale transforms by introducing nonstationary up-sampling operators. Incorporating nonstationarity marks a significant step forward in developing a more flexible and powerful class of nonlinear pyramid transforms. To illustrate this advancement, we presented detailed examples, proved several fundamental properties, and demonstrated the practical benefits of our framework through a specific application focusing on geometric features.

The application clearly highlights the advantages of multiscale analysis, particularly emphasizing the critical role of locality, a key benefit obtained directly from subdivision-based upsampling operators. This inherent locality not only enhances computational efficiency but also improves the framework’s adaptability to varying geometric structures in the data. By leveraging subdivision operators, our method achieves precise representation of geometric details, significantly improving the effectiveness of multiscale analysis.

Our results show that the proposed framework has considerable potential for a wide range of applications in geometric data analysis. While the example presented here primarily serves as an initial demonstration, it effectively showcases flexibility and practical value. The robust and versatile nature of our pyramid-based approach creates numerous opportunities in data processing areas, such as denoising, anomaly detection, feature extraction, image and shape analysis, and data compression. Such broad applicability makes the framework especially appealing for tasks involving geometric and structured data.

Looking ahead, several promising research directions are worth exploring. These include extending our theory to accommodate nonlinear operators, addressing theoretical challenges, and adapting the approach to handle complex, real-world data structures. Future work will also explore applications involving manifolds, Lie groups, graphs, and higher-dimensional data. Additionally, investigating computational improvements and potential integrations with modern machine learning techniques, including deep learning, will further enhance the practical relevance and impact of this research.

Acknowledgement

NS and WM are partially supported by the DFG award 514588180. WM is partially supported by the Nehemia Levzion Scholarship for Outstanding Doctoral Students from the Periphery (2023).

References

- [1] Maria Charina, Costanza Conti, Nicola Guglielmi, and Vladimir Protasov. Limits of level and parameter dependent subdivision schemes: a matrix approach. *Applied Mathematics and Computation*, 272:20–27, 2016.
- [2] Albert Cohen and Nira Dyn. Nonstationary subdivision schemes and multiresolution analysis. *SIAM Journal on Mathematical Analysis*, 27(6):1745–1769, 1996.
- [3] Costanza Conti, Mariantonia Cotronei, Lucia Romani, et al. Beyond b-splines: exponential pseudo-splines and subdivision schemes reproducing exponential polynomials. *Dolomites Research Notes on Approximation*, 10(Special Issue):31–42, 2017.
- [4] Costanza Conti, Laura Gori, and Francesca Pitolli. Totally positive functions through nonstationary subdivision schemes. *Journal of computational and applied mathematics*, 200(1):255–265, 2007.
- [5] Costanza Conti and Lucia Romani. Algebraic conditions on non-stationary subdivision symbols for exponential polynomial reproduction. *Journal of Computational and Applied Mathematics*, 236(4):543–556, 2011.
- [6] Ingrid Daubechies. *Ten lectures on wavelets*. SIAM, 1992.
- [7] Giuliano De Stefano and Oleg V Vasilyev. Hierarchical adaptive eddy-capturing approach for modeling and simulation of turbulent flows. *Fluids*, 6(83), 2021.
- [8] Gilles Deslauriers and Serge Dubuc. Symmetric iterative interpolation processes. *Constructive Approximation: Special Issue: Fractal Approximation*, pages 49–68, 1989.
- [9] David L Donoho. Interpolating wavelet transforms. *Preprint, Department of Statistics, Stanford University*, 2(3):1–54, 1992.
- [10] Nira Dyn. Subdivision schemes in cagd. *Advances in numerical analysis*, 2:36–104, 1992.
- [11] Nira Dyn. Analysis of convergence and smoothness by the formalism of laurent polynomials. In *Tutorials on Multiresolution in Geometric Modelling*, pages 51–68. Springer, 2002.
- [12] Nira Dyn, John A Gregory, and David Levin. Analysis of uniform binary subdivision schemes for curve design. *Constructive Approximation*, 7:127–147, 1991.
- [13] Nira Dyn and David Levin. Analysis of asymptotically equivalent binary subdivision schemes. *Journal of mathematical analysis and applications*, 193(2):594–621, 1995.
- [14] Nira Dyn and David Levin. Subdivision schemes in geometric modelling. *Acta Numerica*, 11:73–144, 2002.
- [15] Nira Dyn, David Levin, and Ariel Luzzatto. Exponentials reproducing subdivision schemes. *Foundations of Computational Mathematics*, 3:187–206, 2003.
- [16] Nira Dyn and Nir Sharon. Manifold-valued subdivision schemes based on geodesic inductive averaging. *Journal of Computational and Applied Mathematics*, 311:54–67, 2017.
- [17] Nira Dyn and Xiaosheng Zhuang. Linear multiscale transforms based on even-reversible subdivision operators. *Excursions in Harmonic Analysis, Volume 6: In Honor of John Benedetto’s 80th Birthday*, pages 297–319, 2021.
- [18] Thomas Gillis and Wim M Van Rees. Murphy—a scalable multiresolution framework for scientific computing on 3d block-structured collocated grids. *SIAM Journal on Scientific Computing*, 44(5):C367–C398, 2022.
- [19] Philipp Grohs. Stability of manifold-valued subdivision schemes and multiscale transformations. *Constructive approximation*, 32:569–596, 2010.
- [20] Ami Harten. Multiresolution representation of data: A general framework. *SIAM Journal on Numerical Analysis*, 33(3):1205–1256, 1996.
- [21] Jinghe Li and Xiangling Wu. Simple framework for the contrastive learning of visual representations-based data-driven tight frame for seismic denoising and interpolation. *Geophysics*, 87(5):V467–V480, 2022.

- [22] Xiupin Lv, Xiaofeng Liao, and Bo Yang. A novel scheme for simultaneous image compression and encryption based on wavelet packet transform and multi-chaotic systems. *Multimedia Tools and Applications*, 77(21):28633–28663, 2018.
- [23] Stéphane Mallat. *A wavelet tour of signal processing*. Elsevier, 1999.
- [24] Wael Mattar and Nir Sharon. Pseudo-reversing and its application for multiscaling of manifold-valued data. *arXiv preprint arXiv:2305.06261*, 2023.
- [25] Wael Mattar and Nir Sharon. Pyramid transform of manifold data via subdivision operators. *IMA Journal of Numerical Analysis*, 43(1):387–413, 2023.
- [26] Wim Sweldens. The lifting scheme: A custom-design construction of biorthogonal wavelets. *Applied and computational harmonic analysis*, 3(2):186–200, 1996.
- [27] Johannes Wallner. Geometric subdivision and multiscale transforms. *Handbook of Variational Methods for Nonlinear Geometric Data*, pages 121–152, 2020.